Journal of Magnetic Resonance 314 (2020) 106721

Contents lists available at ScienceDirect

Journal of Magnetic Resonance

journal homepage: www.elsevier.com/locate/jmr

Slow dynamics of solid proteins – Nuclear magnetic resonance relaxometry versus dielectric spectroscopy

Danuta Kruk [a,*], Elzbieta Masiewicz [a], Milosz Wojciechowski [a], Malgorzata Florek-Wojciechowska [b], Lionel M. Broche [c], David J. Lurie [c]

[a] Faculty of Mathematics and Computer Science, University of Warmia & Mazury in Olsztyn, Słoneczna 54, 10-710 Olsztyn, Poland
[b] Department of Physics & Biophysics, University of Warmia and Mazury in Olsztyn, Oczapowskiego 4, 11-041 Olsztyn, Poland
[c] Bio-Medical Physics, School of Medicine, Medical Sciences & Nutrition, University of Aberdeen, Foresterhill, Aberdeen AB25 2ZD, Scotland, United Kingdom

ARTICLE INFO

Article history:
Received 7 February 2020
Revised 17 March 2020
Accepted 18 March 2020
Available online 19 March 2020

Keywords:
NMR
Relaxation
Relaxometry
Dynamics
Proteins
Dielectric spectroscopy

ABSTRACT

^{1}H Nuclear Magnetic Resonance (NMR) relaxometry and Dielectric Spectroscopy (DS) have been exploited to investigate the dynamics of solid proteins. The experiments have been carried out in the frequency range of about 10 kHz-40 MHz for NMR relaxometry and 10^{-2}Hz-20 MHz for DS. The data sets have been analyzed in terms of theoretical models allowing for a comparison of the correlation times revealed by NMR relaxometry and DS. The ^{1}H spin–lattice relaxation profiles have been decomposed into relaxation contributions associated with ^{1}H–^{1}H and ^{1}H-^{14}N dipole – dipole interactions. The ^{1}H–^{1}H relaxation contribution has been interpreted in terms of three dynamical processes of time scales of 10^{-6}s, 10^{-7}s and 10^{-8}s. It has turned out that the correlation times do not differ much among proteins and they are only weakly dependent on temperature. The analysis of DS relaxation spectra has also revealed three motional processes characterized by correlation times that considerably depend on temperature in contrast to those obtained from the ^{1}H relaxation. This finding suggest that for solid proteins there is a contribution to the ^{1}H spin–lattice relaxation associated with a kind of motion that is not probed in DS as it does not lead to a reorientation of the electric dipole moment.

1. Introduction

Revealing the structure and dynamics of biological macromolecules is essential for understanding their biological function. High resolution Nuclear Magnetic Resonance (NMR) spectroscopy is a leading method providing access to multi-dimensional protein structure and conformation [1–3]. The impressive achievements in terms of determining protein structure by NMR are, however, not accompanied by a parallel, deep knowledge of protein dynamics, especially when it comes to slow motion (long time-scale dynamics). The most powerful methods of probing slow dynamics of biomolecules are NMR relaxometry and Dielectric Spectroscopy (DS). Although both methods provide information about molecular motion, their physical principles are very different: spin relaxation is a quantum–mechanical phenomenon reflecting time scales and mechanisms of stochastic fluctuations of magnetic dipole–dipole interactions between pairs of nuclei, while dielectric relaxation is a fingerprint of reorientation of the electric dipole moment of a molecule in response to electric fields. In this work these methods are exploited to enquire into dynamical properties of solid proteins.

Standard NMR relaxation experiments are performed only at a single resonance frequency (magnetic field) versus temperature. By applying Fast Field-Cycling technology [4–7], frequency-dependent relaxation experiments have become possible. The typically-covered frequency range is from about 1 kHz to 120 MHz (referring to the ^{1}H resonance frequency). This broad frequency range allows probing of motional processes on time scales from ms to ns in a single experiment [8–11]. At low frequencies the spin relaxation is dominated by slow dynamics, while for successively higher frequencies spin interactions mediated by progressively faster motional processes become more efficient. NMR relaxometry is a unique method probing molecular dynamics on the atomic level. The dominant mechanism of ^{1}H relaxation is provided by magnetic dipole–dipole interactions. The interactions stochastically fluctuate in time due to molecular (atomic) motion. According to spin relaxation theory, relaxation rates are given as linear combinations of spectral density functions (Fourier transform of time correlation functions), characterizing the motion modulating the dipole–dipole interactions [12–15]. For proteins

* Corresponding author.
E-mail address: danuta.kruk@matman.uwm.edu.pl (D. Kruk).

https://doi.org/10.1016/j.jmr.2020.106721
1090-7807/

there are two ^{1}H relaxation channels: via ^{1}H–^{1}H and ^{1}H-^{14}N dipole–dipole interactions, respectively. The second relaxation pathway gives rise to Quadrupole Relaxation Enhancement (QRE) effects [16–29]. The energy level structure of ^{1}H is fully determined by its Zeeman interaction. At the same time the energy level structure of ^{14}N originates from a superposition of its Zeeman interaction and quadrupole coupling – *i.e.* a coupling with the electric field gradient tensor at the ^{14}N site, provided the molecular dynamics are slow. When the ^{1}H resonance frequency (the transition frequency between the ^{1}H energy levels) matches one of the ^{14}N transition frequencies, the ^{1}H polarization can be "taken over" by ^{14}N, leading to a frequency-specific enhancement of the ^{1}H spin–lattice relaxation rate referred to as QRE, while the ^{1}H spin–lattice relaxation rate maxima are called quadrupole peaks. The positions of the quadrupole peaks depend on the quadrupole parameters which are determined by the electric field gradient tensor at the ^{14}N site. In consequence, the QRE is a very sensitive fingerprint of molecular arrangement which can be exploited in materials science [19,22–24], biology [25,26], and medicine [27–29].

Dielectric spectroscopy is based on the interaction of an external electric field with the electric dipole moment of the molecule. Dielectric relaxation studies provide information on molecular rotation from the point of view of reorientation of the electric dipole moment of the molecule. The use of DS to probe the motion requires molecules to have a nonzero electric dipole moment. The rotational correlation time probed by DS is a rank-one correlation time describing reorientation of an electric moment of the molecule, while NMR relaxometry gives access to a rank-two correlation time associated with magnetic dipole–dipole interactions between two nuclei. For small-step rotational dynamics the rank-one correlation time is three times longer than its rank-two counterpart. One could argue at this stage that the frequency range accessible by DS is much broader than in NMR relaxometry; indeed, this is the case. It is important to realize, however, that DS does not allow one to enquire into the molecular dynamics on the atomic level – rather, the method traces the reorientation of the overall electric dipole moment. To be more specific, one can say that for small molecules, DS probes the overall molecular rotation. For more complex (larger) molecules such as, for example, polymers, the local segmental dynamics are probed (provided the dipole moment is transverse to the polymer chain) or the backbone reorientation is explored (for polymers in which there is a component of their electric dipole moment parallel to the backbone).

NMR relaxometry studies for solids are rare in general, and even more so for solid biomolecules. Some attention has been devoted to water dynamics in hydrated proteins by NMR relaxometry [30–35]. As far as solid, dry proteins are concerned, one can provide only a few examples of such studies [36–38]. It has been assumed that the shape of the frequency dependence of ^{1}H spin–lattice relaxation in solid proteins can be attributed to structural fluctuations along the backbone [36,37]. In consequence, a power-law model has been developed, with an amplitude reflecting the highest vibrational frequency of the fluctuations and a slope related to their fractal dimensionality [36]. The theory has been revisited [37] by including strong dipole–dipole interactions between the side-chain protons and the protein backbone. An entirely different concept, referred to as a "model-free approach", based on a decomposition of the overall spin–lattice relaxation rates associated with the ^{1}H–^{1}H dipole–dipole relaxation pathway into contributions related to dynamical processes occurring on different time scales has been proposed in [39]. This model has been employed for the analysis of ^{1}H spin–lattice relaxation data for proteins in water solution [34,35], in sediments [40] as well as for polymers [41]. The concept has recently been exploited by us to reveal and compare the multi-scale dynamics of Bovine Serum Albumin (BSA), Albumin from Human Plasma (AHP), Elastin from bovine neck ligament and Lysozyme from hen egg white in the solid state (powder) form [38]. The studies have, however, been performed only at a single temperature of 308 K.

As far as DS studies of solid biomolecules are concerned, one can provide a few examples of such results [42–45], but the data are mostly used as a reference point to investigate, in fact, water dynamics in the systems [46–49].

Comparisons of NMR relaxometry and DS results have very seldom been performed and they are limited to simple molecules [50,51]; there are perhaps two reasons for this situation. The first one lies in the novelty of NMR relaxometry in comparison to the well-established DS. The second reason is the complex, quantum–mechanical foundation of spin relaxation – a deep knowledge of the theory of spin relaxation is required to properly separate quantum–mechanical (resulting from an interplay between spin interactions) and dynamical (resulting from molecular dynamics) components of the relaxation processes.

To profit from the potential of joint (complementary) studies of molecular dynamics by means of NMR relaxometry and DS, well justified links between the outputs of both methods must be established. Developing a methodology of comparing spin and dielectric relaxation processes in terms of the underlying molecular dynamics constitutes the first goal of this paper. The second goal is to undertake the challenge of providing a consistent interpretation of NMR relaxometry and DS data (taking into account the different physical background of the two methods) in order to deeply enquire into dynamics of solid proteins occurring on a long time scale. To our knowledge, the presented studies are the first example of combining NMR relaxometry and DS for investigating the dynamics of macromolecules.

The paper is organized as follows. In Section 2 (2.1 and 2.2), the theoretical foundation of ^{1}H relaxation processes in solids and DS is presented – special attention has been turned to a development of a methodology allowing for a comparison of experimental data obtained by means of these two methods. Section 2.3 includes experimental details, while in Section 3 the experimental data are presented, analysed, discussed. Eventually, Section 4 contains concluding remarks.

2. Materials and methods

2.1. Theory: ^{1}H spin–lattice relaxation dispersion profiles

^{1}H spin–lattice relaxation for proteins is caused by ^{1}H–^{1}H and ^{1}H-^{14}N magnetic dipole–dipole interactions. Consequently, the overall ^{1}H spin–lattice relaxation rate, $R_1(\omega_H)$ (ω_H denotes the ^{1}H resonance frequency in angular frequency units) is a sum of the corresponding relaxation rates $R_1^{HH}(\omega_H)$ and $R_1^{HN}(\omega_H)$:

$$R_1(\omega_H) = R_1^{HH}(\omega_H) + R_1^{HN}(\omega_H) \tag{1}$$

In the case of a homogenous (characterized by a single correlation time) dynamics modulating the dipole–dipole interactions and leading to a single-exponential correlation function, the $R_1^{HH}(\omega_H)$ relaxation contribution is given as [12–15]:

$$R_1^{HH}(\omega_H) = C^{HH}[J(\omega_H) + 4J(2\omega_H)] = C^{HH}\left[\frac{\tau_c}{1+(\omega_H\tau_c)^2} + \frac{4\tau_c}{1+(2\omega_H\tau_c)^2}\right] \tag{2}$$

where τ_c denotes the correlation time of this dynamical process, while C^{HH} is referred to as a dipolar relaxation constant; it is defined as: $C^{HH} = \frac{3}{10}\left(\frac{\mu_0}{4\pi}\frac{\gamma_H^2\hbar}{r_{HH}^3}\right)^2$, where γ_H denotes the ^{1}H gyromagnetic factor, while r_{HH} should be treated as an "effective" inter-spin distance

accounting for dipole–dipole interactions between several pairs of protons. The spectral density function, $J(\omega)=\frac{\tau_c}{1+(\omega\tau_c)^2}$, can be transformed to the co-called susceptibility representation by multiplying it with ω (the $\varepsilon_{NMR}(\omega,\tau_c)$ function then takes the Debye form given by Eq. (3)):

$$\varepsilon_{NMR}(\omega,\tau_c)=\omega J(\omega)=\frac{\omega\tau_c}{1+(\omega\tau_c)^2} \tag{3}$$

This implies that the ^{1}H spin–lattice relaxation rates (Eq. (2)) can be expressed in the susceptibility representation as:

$$\begin{aligned}\chi_{NMR}(\omega_H,\tau_c)&=\omega_H R_1^{HH}(\omega_H)\\&=C^{HH}[\varepsilon_{NMR}(\omega_H,\tau_c)+2\varepsilon_{NMR}(2\omega_H,\tau_c)]\end{aligned} \tag{4}$$

NMR relaxation studies performed as a function of frequency give access to dynamical processes of different time scales. Relaxation contributions associated with slow dynamics dominate the relaxation at low frequencies, then, with increasing frequency, relaxation terms originating from fast fluctuations of the dipole–dipole interactions become progressively more pronounced. Anticipating the results, the $R_1^{HH}(\omega_H)$relaxation rates for solid proteins can be expressed as a sum of the following terms [38]:

$$\begin{aligned}R_1^{HH}(\omega_H)\;&=C_s^{HH}\left[\frac{\tau_s^{(2)}}{1+\left(\omega_H\tau_s^{(2)}\right)^2}+\frac{4\tau_s^{(2)}}{1+\left(2\omega_H\tau_s^{(2)}\right)^2}\right]+C_i^{HH}\left[\frac{\tau_i^{(2)}}{1+\left(\omega_H\tau_i^{(2)}\right)^2}+\frac{4\tau_i^{(2)}}{1+\left(2\omega_H\tau_i^{(2)}\right)^2}\right]\\&+C_f^{HH}\left[\frac{\tau_f^{(2)}}{1+\left(\omega_H\tau_f^{(2)}\right)^2}+\frac{4\tau_f^{(2)}}{1+\left(2\omega_H\tau_f^{(2)}\right)^2}\right]+A\end{aligned} \tag{5}$$

where the pairs of parameters, $\left(C_s^{HH},\tau_s^{(2)}\right)$, $\left(C_i^{HH},\tau_i^{(2)}\right)$, $\left(C_f^{HH},\tau_f^{(2)}\right)$ refer to slow, intermediate and fast dynamical processes, while the frequency-independent term, A, describes a relaxation contribution associated with dynamics of a time-scale shorter than 10^{-9}s. For such short correlation times the condition $\omega_H\tau_c<<1$ holds and, therefore, the corresponding relaxation rate does not show a dependence on ω_H. The index (2) in the correlation times, $\tau_s^{(2)}$, $\tau_i^{(2)}$, $\tau_f^{(2)}$, explicitly points out that the quantities are rank-two correlation times, as magnetic dipole–dipole interactions are rank-two spin interactions. For convenience we shall refer to the first, second and third terms of Eq. (5) as: $R_{1,s}^{HH}$, $R_{1,i}^{HH}$ and $R_{1,f}^{HH}$, respectively. In analogy to Eq. (4) one can transform Eq. (5) to the susceptibility representation:

$$\begin{aligned}\chi_{NMR}=\chi_{NMR,s}+\chi_{NMR,i}+\chi_{NMR,f}&=C_s^{HH}\left[\varepsilon_{NMR}(\omega_H,\tau_s^{(2)})\right.\\&\left.+2\varepsilon_{NMR}(2\omega_H,\tau_s^{(2)})\right]+C_i^{HH}\left[\varepsilon_{NMR}\left(\omega_H,\tau_i^{(2)}\right)+2\varepsilon_{NMR}\left(2\omega_H,\tau_i^{(2)}\right)\right]\\&+C_{sf}^{HH}\left[\varepsilon_{NMR}\left(\omega_H,\tau_f^{(2)}\right)+2\varepsilon_{NMR}\left(2\omega_H,\tau_f^{(2)}\right)\right]+A\omega_H\end{aligned} \tag{6}$$

As far as the ^{1}H-^{14}N relaxation contribution is concerned, the $R_1^{HN}(\omega_H)$ relaxation rate can be expressed as in terms of Eq. (4) of [38], based on [51]. The model predicts the existence of three frequency specific relaxation maxima referred to as quadrupole peaks caused by the QRE effects [16–29,51]. The quadrupole peaks appear at the frequencies: $\nu_-=\frac{\omega_-}{2\pi}=\frac{3}{4}a_Q\left(1-\frac{\eta}{3}\right)$, $\nu_+=\frac{\omega_+}{2\pi}=\frac{3}{4}a_Q\left(1+\frac{\eta}{3}\right)$ and $\nu_0=\nu_+-\nu_-=\frac{\omega_0}{2\pi}=\frac{1}{2}\eta\,a_Q$, where a_Q and η describe the amplitude and the asymmetry parameter of the quadrupole coupling, respectively. The amplitude is defined as: $a_Q=e^2qQ/\hbar$, where Q denotes the quadrupole moment of the nucleus, while q is the zz component of the electric field gradient tensor at its site. The model also involves angles Θ andΦ describing the orientation of the ^{1}H-^{14}N dipole–dipole axis with respect to the principal axis system of the electric field gradient at the ^{14}N site, a correlation time τ_Q characterizing fluctuations of the ^{1}H-^{14}N dipole–dipole coupling and the ^{1}H-^{14}N inter-spin distance, r_{HN}.

2.2. Dielectric relaxation spectra

Keeping a close analogy between the labeling of NMR and DS quantities (although the labeling somewhat differs from the traditional nomenclature of DS), dielectric relaxation spectra can be modeled in terms of the Cole-Davidson function [53]:

$$\chi_{DS}=C_{DS}\varepsilon_{DS}(\omega,\tau_c^{(1)})=C_{DS}\frac{\sin\left[\beta\arctan\left(\omega\left(\tau_c^{(1)}/\beta\right)\right)\right]}{\left[1+\left(\omega\left(\tau_c^{(1)}/\beta\right)\right)^2\right]^{\beta/2}} \tag{7}$$

There are other functions used in DS for this purpose, for instance Cole-Cole or Havriliak-Negami functions [53–55], but the Cole-Davidson form has been chosen here, anticipating the DS results for solid proteins. The parameter β is in the range of $0<\beta\leqslant 1$; for $\beta=1$ the Cole-Davidson function converges to the Debye form. For $\beta<1$ the Cole-Davidson function becomes broader on the high frequency site compared to the Debye function. This implies a distribution of correlation times (*i.e.* heterogeneous dynamics). It is of primary importance to note that the correlation time, $\tau_c^{(1)}$, probed in DS is a rank-one correlation function. For small step rotational dynamics the relationship $\tau_c^{(1)}=3\tau_c^{(2)}$holds. The pre-factor C_{DS} (a dielectric relaxation constant) in Eq. (7) describes the amplitude of the dielectric relaxation peak.

Anticipating further the experimental results, the dielectric relaxation spectra can be described in terms of three relaxation peaks of the Cole-Davidson shape:

$$\begin{aligned}\chi_{DS}&=C_{DS,es}\varepsilon_{DS,es}(\omega,\tau_{es}^{(1)})+C_{DS,s}\varepsilon_{DS,s}(\omega,\tau_s^{(1)})+C_{DS,i}\varepsilon_{DS,i}\left(\omega,\tau_i^{(1)}\right)\\&+B\omega^{-\alpha}=C_{DS,es}\frac{\sin\left[\beta_{es}\arctan\left(\omega\left(\tau_{es}^{(1)}/\beta_{es}\right)\right)\right]}{\left[1+\left(\omega\left(\tau_{es}^{(1)}/\beta_{es}\right)\right)^2\right]^{\beta_{es}/2}}\\&+C_{DS,s}\frac{\sin\left[\beta_s\arctan\left(\omega\left(\tau_s^{(1)}/\beta_s\right)\right)\right]}{\left[1+\left(\omega\left(\tau_s^{(1)}/\beta_s\right)\right)^2\right]^{\beta_s/2}}+C_{DS,i}\frac{\sin\left[\beta_i\arctan\left(\omega\left(\tau_i^{(1)}/\beta_i\right)\right)\right]}{\left[1+\left(\omega\left(\tau_i^{(1)}/\beta_i\right)\right)^2\right]^{\beta_i/2}}+B\omega^{-\alpha}\end{aligned} \tag{8}$$

The indexes "es", "s" and "i" refer to extra-slow, slow and intermediate dynamics. The labeling is meant to match the time scale of the dynamical processes revealed in the NMR relaxometry experiments. The "classification" of the time scales of the dynamical processes can be somewhat problematic – in principle, one could ask why Eq. (8) does not refer to slow, intermediate and fast dynamics, in analogy to Eq. (6). Anticipating the results, we can say that the fast dynamics identified in the analysis of the ^{1}H spin–lattice relaxation dispersion profiles is characterized by correlation times of the order of 10^{-8}s; so fast processes are not seen in the dielectric experiments in the considered frequency range. The parameters B and αcharacterize the conductivity contribution to the dielectric relaxation spectra.

2.3. Experimental details

^{1}H spin–lattice relaxation experiments were performed in the frequency range from 4 kHz to 30 MHz (referring to ^{1}H resonance frequency) using an FFC relaxometer (Stelar S.r.l., Mede, Italy, Spinmaster 2000). For frequencies above 10 MHz initial prepolarization at 25 MHz has been applied (expressing the magnetic field as the equivalent ^{1}H resonance frequency). The duration of the radio-frequency pulse was 8 μs, the detection frequency was

15.8 MHz, the slew rate of the magnetic field was 12 MHz/ms and the repetition delay time was five times larger than the spin–lattice relaxation time at the frequency of 30 MHz. The ^{1}H magnetization curves were recorded with 8 accumulations for 16 logarithmically-spaced time intervals. Temperature was controlled with an accuracy of 0.5 K. The relaxation process turned out to be single-exponential for all proteins at all temperatures in the whole frequency range.

DS measurements were performed using a Novocontrol impedance analyzer operating in the frequency range from 10 − 2 Hz to 20 MHz. Temperature was controlled using a nitrogen gas cryostat with an accuracy of 0.5 K. The measurements were conducted using a parallel-plate steel capacitor of 20 mm diameter.

The proteins studied were as follows: Elastin from bovine neck ligament, Lysozyme from hen egg white, Bovine Serum Albumin (BSA) and Myoglobin from equine heart were purchased from Sigma-Aldrich in the form of lyophilized powder. In addition, ^{1}H spin–lattice relaxation measurements for hydrated elastin (10% wt and 37%wt of water) and hydrated lysozyme (24%wt of water) were performed for comparison. The essential structural properties of the first three proteins have been outlined in [38]. BSA and lysozyme are globular, while elastin is a fibrillar protein. Molecular weights of BSA is 66.4 kDa [56], the number of amino acids: 583 [57]. The helical content of BSA reaches 53%, 14% of BSA structure forms β- sheets, 4% forms β- turns and 16% is random [58]. The molecular weight of lysozyme is 13.9 kDa.; the α- helical content ranges from 26 to 31 % and β structure content varies between 11 and 16% [59,60]. The elastin monomer, tropoelastin, weights about 70 kDa, the helical content of elastin is about 10%, while about 35% of the structure forms β- strands [61,62]. Myoglobin is also a globular protein; its molecular weight is 16.7KDa. It contains 154 amino acids and consists of eight alpha helices. Myoglobin contains a porphyrin ring with an iron at its centre and attached histidine groups [63,64].

3. Results and discussion

3.1. ^{1}H spin–lattice NMR relaxation dispersion profiles

The ^{1}H spin–lattice relaxation profiles for the solid proteins: bovine Elastin (293 K, 312 K), Lysozyme from hen egg white (293 K, 363 K), BSA (233 K) and Myoglobin from equine heart (293 K) are shown in Fig. 1. The data for Lysozyme and BSA are in good agreement with those reported in [65] at 302 K, although

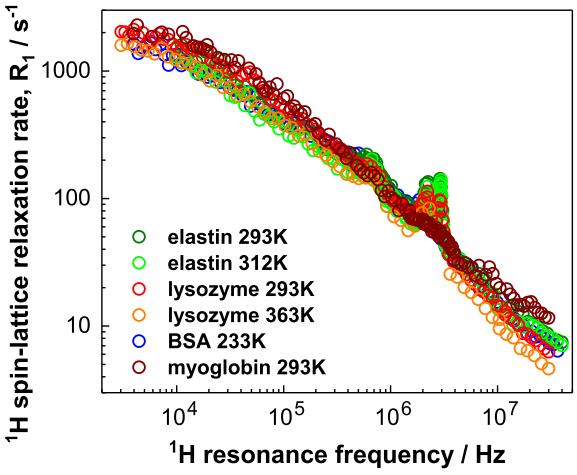

Fig. 1. ^{1}H spin–lattice relaxation dispersion profiles for solid proteins. The data are very similar for all proteins and only weakly dependent on temperature.

in the present case the QRE effects have been investigated in much more detail.

The first observation is that the relaxation profiles do not differ much. They only slightly change with temperature. The data for bovine elastin, lysozyme and BSA at 308 K shown in [38] confirm this statement. Moreover, the relaxation profiles are similar for all proteins, despite their different structures. The last statement should, however, be treated with caution: contrary to the other proteins, myoglobin does not show QRE effects.

The NMR relaxation data have been analyzed in terms of Eq. (1) with $R_1^{HH}(\omega_H)$ described by Eq. (5) and $R_1^{HN}(\omega_H)$. For myoglobin the $R_1^{HN}(\omega_H)$relaxation contribution has been omitted. The result of the analysis is shown in Fig. 2. The obtained parameters are collected in Table 1.

The correlation times characterizing the slow dynamical process, $\tau_s^{(2)}$, varies between 2.33 * 10^{-6}s and 3.86 * 10^{-6}s (the ratio between the correlation times is below 2). The correlation times $\tau_i^{(2)}$ and $\tau_f^{(2)}$ do not vary much either; $\tau_i^{(2)}$ ranges between 1.23 * 10^{-7}s and 3.09 * 10^{-7}s, while for $\tau_f^{(2)}$ the span reaches 6.32 * 10^{-9}s – 2.09 * 10^{-8}s. Analogously, the corresponding dipolar relaxation constants show only small variations between the proteins. The frequency independent term, A, can be attributed to the fast dynamics of methyl groups. The quadrupole parameters, a_Q and η, have been determined from the positions of the QRE maxima (quadrupole peaks). They are similar for elastin, lysozyme and BSA. This is not surprising taking into account that the protein backbones in all proteins have the same local structure and the ^{1}H-^{14}N relaxation contribution stems from ^{1}H-^{14}N dipole–dipole interactions in the protein backbone amide groups. The correlation times, τ_Q, characterizing the fluctuations of the ^{1}H-^{14}N dipole – dipole coupling are also very similar for all proteins; the correlation times are in all cases somewhat shorter than $\tau_s^{(2)}$, but longer than $\tau_i^{(2)}$. The effective fluctuations of the ^{1}H-^{14}N dipole–dipole interactions originate from the molecular dynamics and the quadrupole relaxation of ^{14}N. The second contribution leads to a shortening of the effective correlation time. One can also expect ^{1}H-^{14}N relaxation contributions associated with the intermediate and fast dynamics. Quadrupole peaks are, however, observed only for slow dynamics. This implies that one can hardly reveal possible ^{1}H-^{14}N relaxation contributions associated with a relatively fast motion, especially as the terms are small (γ_N is small) – they are masked by the ^{1}H–^{1}H relaxation contributions. The ^{1}H-^{14}N inter-spin distance is longer than the one reported in the literature [66] the ^{1}H-^{14}N bound length in amide groups (about 1 Å). The same situation has been reported in [38]. One should, however, take into account that Eq. (4) of Ref. [38] describes QRE effects for a system including one ^{1}H and one ^{14}N nuclei. Considering more nuclei into the description would mean including numerous (unknown) parameters. Though, there are longer-range dipole–dipole couplings between non-bonded ^{1}H and ^{14}N nuclei contributing to the effect. Furthermore, the ratio between the number of involved ^{1}H and ^{14}N nuclei is not 1:1. To understand why QRE effects are not seen for myoglobin one should realize that in this compound paramagnetic Fe centres are placed in the vicinity of ^{14}N nuclei. The fast electronic relaxation acts as an additional source of the ^{14}N relaxation, leading to a broadening (in fact, to the extent of disappearance) of the quadrupole peaks. In other words: the ^{1}H-^{14}N dipole–dipole coupling fluctuates in time as a result of the protein dynamics and the ^{14}N relaxation that originates from two sources: local fluctuations of the electric field gradient tensor and dipole–dipole interactions between ^{14}N and the electron spin of the paramagnetic center. The second contribution can make the ^{14}N relaxation fast, shortening the effective correlation time, τ_Q

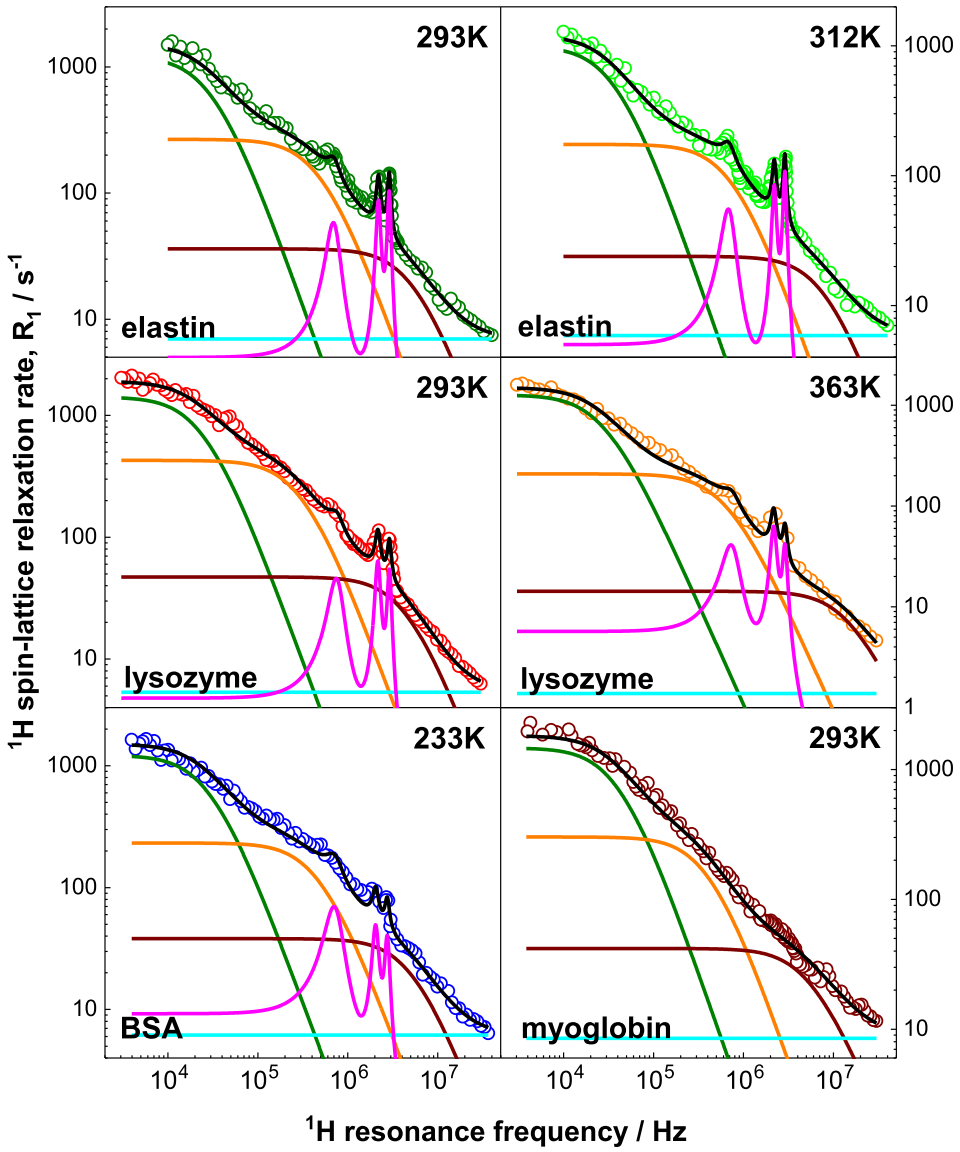

Fig. 2. ^{1}H spin–lattice relaxation rates, R_1^{HH}; black lines – theoretical fits decomposed into the individual relaxation contributions: $R_{1,s}^{HH}$ (green lines), $R_{1,i}^{HH}$ (orange lines), $R_{1,f}^{HH}$ (brown lines),A (light blue lines) andR_1^{HN}(pink lines). (For interpretation of the references to color in this figure legend, the reader is referred to the web version of this article.)

Table 1
Parameters obtained from the analysis of the ^{1}H spin–lattice relaxation data, $^{(+)}$ - not adjustable parameters.

parameter	elastin		lysozyme		BSA	myoglobin
T / K	293	312	293	363	233	293
C_s^{HH}/ Hz^2	7.85 * 10^7		7.33 * 10^7		7.43 * 10^7	1.26 * 10^8
$\tau_s^{(2)}$/ s	3.09 * 10^{-6}	2.53 * 10^{-6}	3.86 * 10^{-6}	3.46 * 10^{-6}	3.28 * 10^{-6}	2.33 * 10^{-6}
C_i^{HH}/ Hz^2	2.84 * 10^8		2.77 * 10^8		2.36 * 10^8	2.63 * 10^8
$\tau_i^{(2)}$/ s	1.88 * 10^{-7}	1.23 * 10^{-7}	3.09 * 10^{-7}	1.51 * 10^{-7}	1.97 * 10^{-7}	2.30 * 10^{-7}
C_f^{HH}/ Hz^2	4.21 * 10^8		4.52 * 10^8		4.31 * 10^8	6.31 * 10^8
$\tau_f^{(2)}$/ s	1.72 * 10^{-8}	1.14 * 10^{-8}	2.09 * 10^{-8}	6.32 * 10^{-9}	1.77 * 10^{-8}	1.80 * 10^{-8}
A/ s^{-1}	6.97	5.87	5.34	1.38	6.18	8.60
$^{(+)}$ a_Q/ MHz	3.38		3.37		3.18	–
$^{(+)}$ η	0.41	0.40	0.44	0.43	0.44	–
τ_Q/ s	1.21 * 10^{-6}	1.20 * 10^{-6}	1.01 * 10^{-6}	8.82 * 10^{-7}	8.89 * 10^{-7}	–
r_{HN}/ Å	1.64	1.64	1.71	1.71	1.69	–
Θ/ °	69	70	62	61	41	–
Φ/ °	50	52	41	33	38	–
rel. error (%)	7.4	7.3	5.8	9.4	8.4	7.9

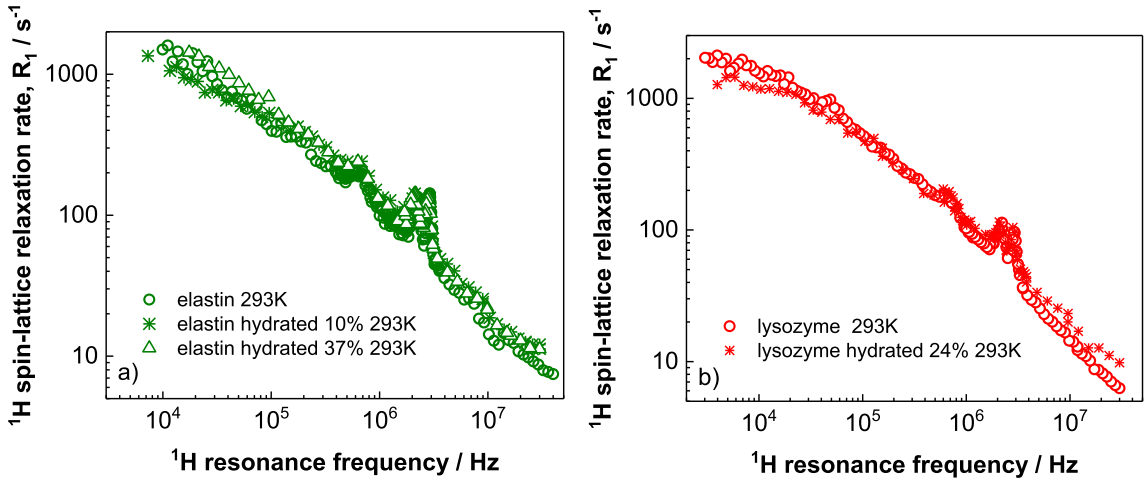

Fig. 3. ^{1}H spin–lattice relaxation rates, R_1^{HH}, for hydrated elastin (a)) and hydrated lysozyme (b)) at 293 K; for comparison the corresponding data for the non-hydrated proteins (taken from Fig. 1) are shown.

and, hence, leading to the condition: $2\pi a_Q \tau_Q \ll 1$being fulfilled. In such a case one does not observe QRE effects.

It is interesting to mention that a large amount of water is needed for the protein dynamics to change. Fig. 3 shows ^{1}H spin–lattice relaxation dispersion profiles for hydrated elastin and lysozyme. Even the hydration level is high (37%wt for elastin and 24%wt for lysozyme), the differences between the shapes of the relaxation data are not significant.

3.2. Dielectric relaxation spectra

The dielectric relaxation spectra for bovine Elastin, Lysozyme from hen egg white, BSA and Myoglobin from equine heart are shown in Fig. 4. The color scheme has been chosen to match the colors of the corresponding NMR relaxation profiles.

Before proceeding with the analysis the spectra were normalized (the amplitude of the maxima being set to unity) and displayed in Fig. 5. The spectra for which there is no maximum present in the discussed frequency range have been omitted (lysozyme and BSA at 293 K and 312 K).

In order to compare the results of NMR relaxometry and DS, a sum of the NMR susceptibility functions $\varepsilon_{NMR}\left(\omega,\tau_s^{(1)}\right)$, $\varepsilon_{NMR}\left(\omega,\tau_i^{(1)}\right)$ and $\varepsilon_{NMR}\left(\omega,\tau_f^{(1)}\right)$ (where $\omega_H$has been replaced byω for simplicity) for$\tau_s^{(1)}=3\tau_s^{(2)}$, $\tau_i^{(1)}=3\tau_i^{(2)}$ and $\tau_f^{(1)}=3\tau_f^{(2)}$ (using the values of$\tau_s^{(2)}$, $\tau_i^{(2)}$ and$\tau_f^{(2)}$ obtained from the analysis of the ^{1}H spin–lattice relaxation dispersion profiles) has been plotted in Fig. 6a,b for elastin at 293 K and 312 K. The ratios between the amplitudes of the relaxation peaks have been set as equal to the ratios between the corresponding dipolar relaxation constants. It has turned out that although shifted towards high frequencies, the resulting peaks capture some features of the dielectric relaxation spectra. Following Eq. (8) one can reproduce the dielectric relaxation spectra in terms of three Cole-Davidson contributions as shown in Fig. 6c, d. The analysis has revealed a relaxation peak

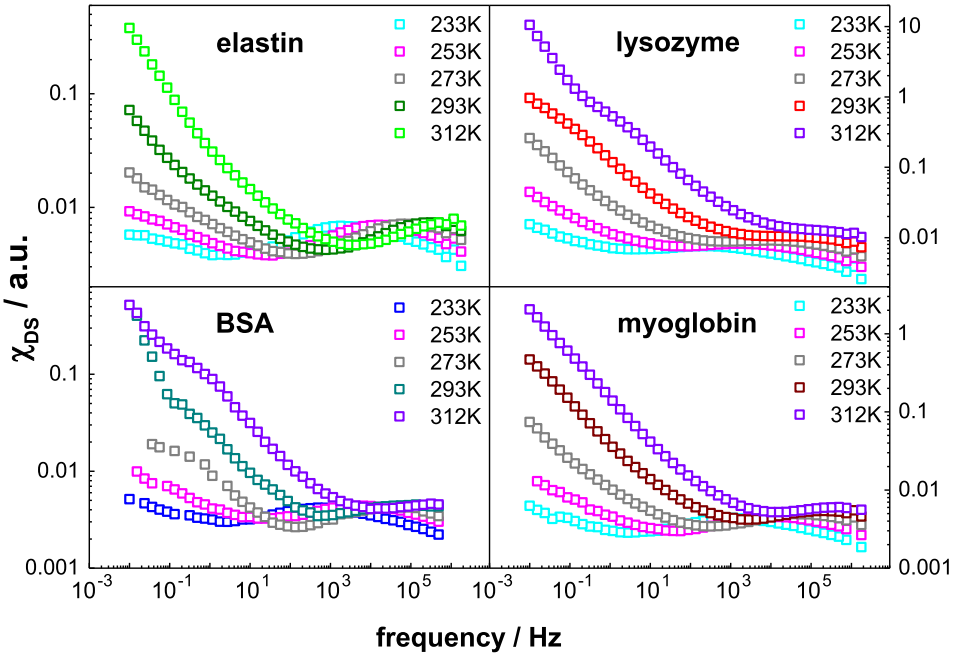

Fig. 4. Dielectric relaxation spectra, $\chi_{DS}(\omega)$, for solid elastin, lysozyme, BSA and myoglobin.

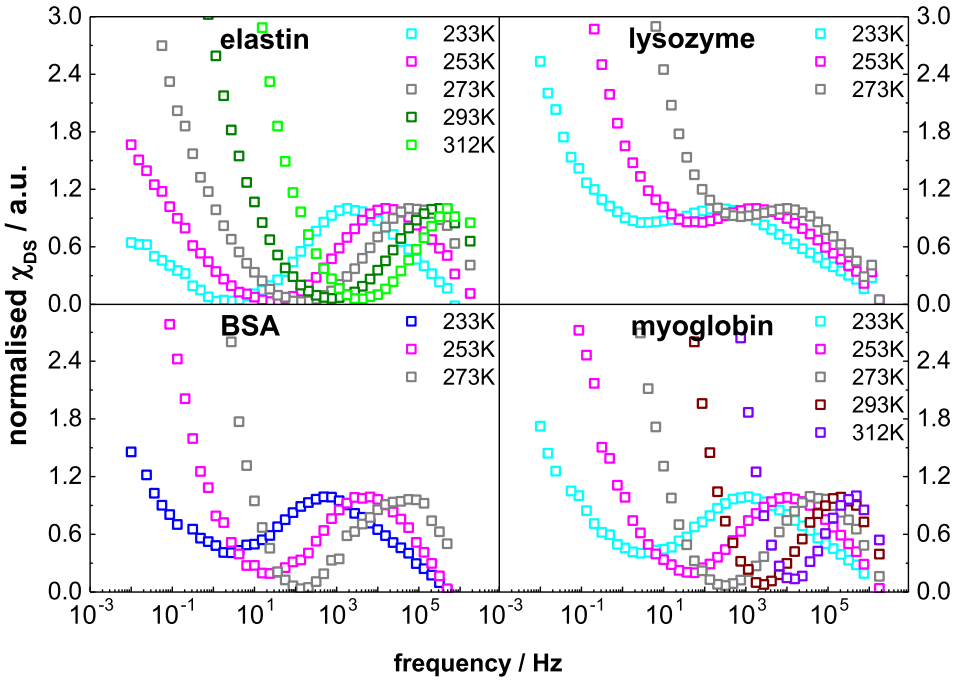

Fig. 5. Dielectric relaxation spectra, $\chi_{DS}(\omega)$, for solid elastin, lysozyme, BSA and myoglobin were normalized in such a way so the maxima of the dielectric relaxation peaks reached the value of 1.

at very low frequencies, masked by the conductivity term – the corresponding correlation time has been denoted as $\tau_{es}^{(1)}$ (as anticipated in Eq. (8)). The obtained parameters are collected in Table 2.

The dielectric spectra can, however, be also quite well reproduced in terms of three motional processes with the correlations times $\tau_s^{(1)} = 3\tau_s^{(2)}$, $\tau_i^{(1)} = 3\tau_i^{(2)}$ and $\tau_f^{(1)} = 3\tau_f^{(2)}$ (where $\tau_s^{(2)}$, $\tau_i^{(2)}$ and $\tau_f^{(2)}$ are obtained from the analysis of the ^{1}H spin–lattice relaxation dispersion profiles) by adjusting their relative contributions, *i.e.* the C_s^{HH}, C_i^{HH} and C_f^{HH} parameters as shown in Fig. 6e,f. The concept of interpreting the dielectric relaxation spectra in terms of Eq. (8) has also been applied to the dielectric data for solid elastin at 273 K, 253 K and 233 K. The results are shown in Fig. 7a-c, while the obtained parameters are collected in Table 2. At these temperatures the extra slow process is masked by the conductivity (the conductivity contribution is not explicitly shown but included into the overall fit). The parameters $C_{DS,es}$, $C_{DS,s}$ and $C_{DS,i}$ have remained unchanged. Following this concept, the corresponding dielectric spectra for lysozyme at 273 K, 253 K and 233 K have also been interpreted in terms of Eq. (8) as shown in Fig. 7d-e. The obtained parameters are collected in Table 3. For lysozyme one cannot compare the dielectric relaxation spectrum at 293 K with the corresponding susceptibility curves for the correlation times obtained from the analysis of the ^{1}H spin–lattice relaxation dispersion profile, because at this temperature the maximum of the dielectric relaxation spectrum is not visible in the considered frequency range.

The correlation times, $\tau_s^{(1)}$, $\tau_i^{(1)}$and $\tau_s^{(2)}$, $\tau_i^{(2)}$for elastin and lysozyme are plotted versus reciprocal temperature in Fig. 8a, b. In addition, the correlation times obtained in [38] for elastin and lysozyme at 308 K have been included in the figure.

Comparing the dielectric relaxation spectrum for BSA at 233 K (Fig. 9a) with the susceptibility curves corresponding to the parameters obtained from the analysis of the ^{1}H spin–lattice relaxation data, one can easily see that the dielectric spectrum cannot be reproduced in terms of the correlation times $\tau_s^{(1)} = 3\tau_s^{(2)}$, $\tau_i^{(1)} = 3\tau_i^{(2)}$ and $\tau_f^{(1)} = 3\tau_f^{(2)}$ by adjusting the relative contributions of these processes. However, in analogy to elastin and lysozyme, the dielectric spectra for BSA at 233 K, 253 K and 273 K have been analyzed in terms of Eq. (8) (Fig. 9b-d); the obtained parameters are included in Table 4.

Fig. 8c shows the comparison of the correlation times $\tau_s^{(1)}$, $\tau_i^{(1)}$and $\tau_s^{(2)}$, $\tau_i^{(2)}$for BSA including the values for 308 K taken from [38].

As far as myoglobin is concerned, in the first step (in analogy to elastin) a sum of the NMR susceptibility functions $\varepsilon_{NMR}\left(\omega, \tau_s^{(1)}\right)$, $\varepsilon_{NMR}\left(\omega, \tau_i^{(1)}\right)$ and $\varepsilon_{NMR}\left(\omega, \tau_f^{(1)}\right)$ for $\tau_s^{(1)} = 3\tau_s^{(2)}$, $\tau_i^{(1)} = 3\tau_i^{(2)}$ and $\tau_f^{(1)} = 3\tau_f^{(2)}$ (using the values of $\tau_s^{(2)}$, $\tau_i^{(2)}$ and $\tau_f^{(2)}$ obtained from the analysis of the ^{1}H spin–lattice relaxation dispersion profiles) has been compared in Fig. 11a with the normalized dielectric spectrum at 293 K, keeping the ratios between the amplitudes of the relaxation peaks equal to those between the corresponding dipolar relaxation constants. The resulting peak is shifted, analogous to the case of elastin. Fig. 11b shows the result of reproducing the dielectric spectrum in terms of Eq. (8), including the extra-slow and slow processes. Looking at the figure one can wonder why the two Cole-Davidson contributions have not been attributed to the slow and intermediate processes, respectively. As already explained, the labelling is not straightforward, but to make it easier we have chosen to refer to fast dynamics only when the corresponding correlation time is of the order of 10^{-8}s or shorter. The obtained parameters are collected in Table 5. Then, in Fig. 10c the dielectric spectrum has been reproduced, keeping the correlation times obtained from the analysis of the ^{1}H spin–lattice relaxation data, but adjusting the contributions of the corresponding susceptibility curves, by changing the amplitudes C_s^{HH}, C_i^{HH} and C_f^{HH}.

The dielectric relaxation spectra for myoglobin for the remaining temperatures, 312 K, 273 K, 253 K and 233 K, decomposed into the individual Cole-Davidson contributions are shown in Fig. 11. For 312 K only the extra slow and slow processes are visible (in analogy to 293 K), at the lower temperatures, 273 K, 253 K and 233 K, the contribution associated with the intermediate dynamics

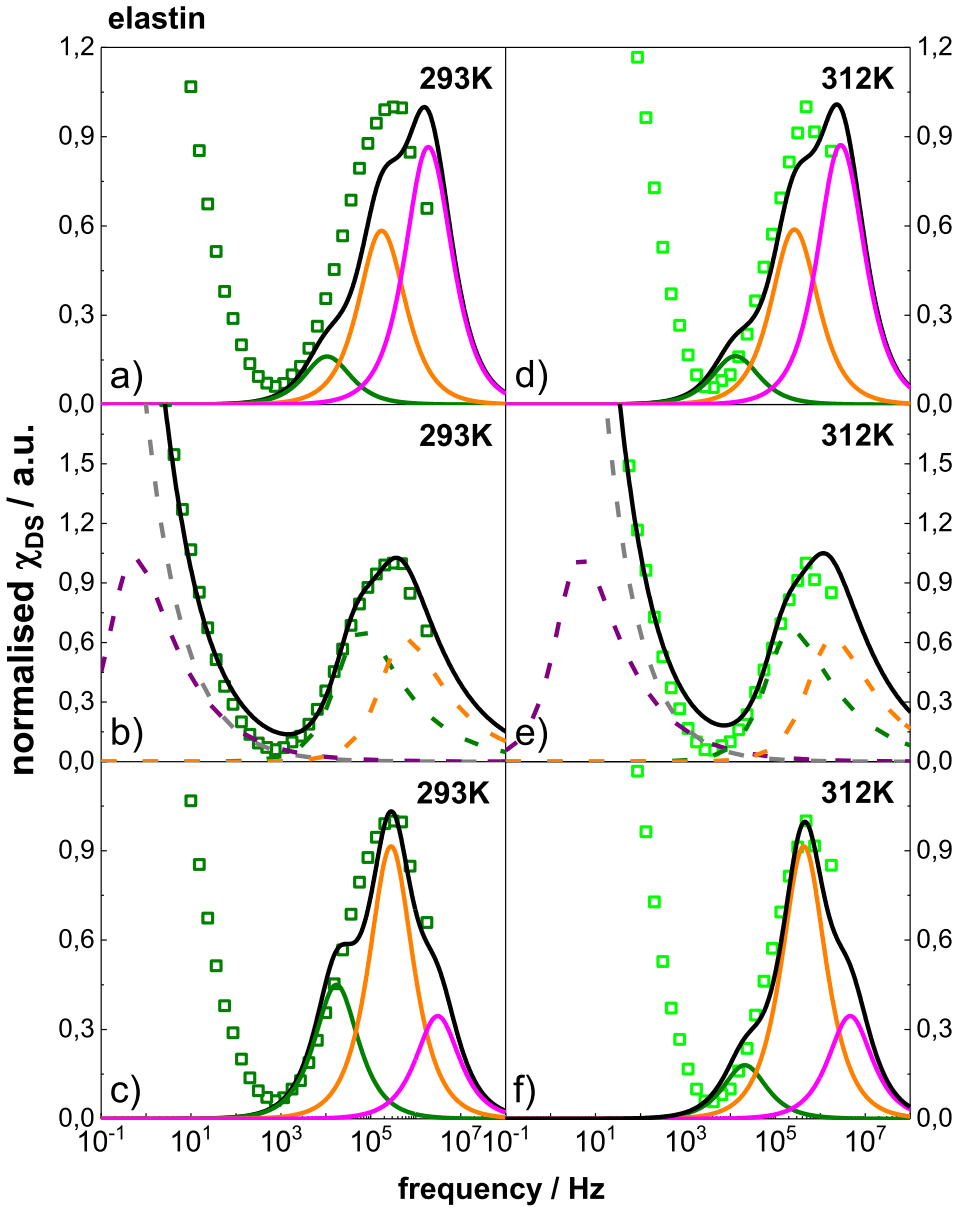

Fig. 6. (a), (b): Normalized dielectric relaxation spectra for elastin at 293 K and 312 K, respectively, compared with the $R_1^{HH}(\omega_H)$ relaxation contribution in the susceptibility representation (χ_{NMR}) decomposed into $R_{1,s}^{HH}$(green solid line), $R_{1,i}^{HH}$ (orange solid line) and$R_{1,f}^{HH}$ (pink solid line) relaxation rates (corresponding to $\chi_{NMR,s}$, $\chi_{NMR,i}$ and $\chi_{NMR,f}$, respectively); (c), (d): normalized $\chi_{DS}(\omega)$ reproduced in terms of Eq. (8) and decomposed into the individual contributions – conductivity (grey dashed line), extra slow process (purple dashed line), slow process (green dashed line) and intermediate process (orange dashed line); (e), (f) normalized $\chi_{DS}(\omega)$ reproduced as a sum of processes contributing to the $R_1^{HH}(\omega_H)$ relaxation terms ($\beta_s = \beta_i = \beta_f = 1$), but with the adjusted pre-factors - C_s^{HH}/C_i^{HH} = 0.49, C_i^{HH}/C_f^{HH} = 2.65 (293 K), C_s^{HH}/C_i^{HH} = 0.20, C_i^{HH}/C_f^{HH} = 2.65 (312 K); black solid lines – overall fits. (For interpretation of the references to color in this figure legend, the reader is referred to the web version of this article.)

Table 2
Parameters obtained from the analysis of dielectric relaxation spectra for elastin. $C_{DS,es}/C_{DS,s}$ = 1.51, $C_{DS,s}/C_{DS,i}$ = 1.10.

T / K	233	253	273	293	312
$\tau_{es}^{(1)}$/ s	–	–	–	0.58	0.07
β_{es}	–	–	–	0.42	0.42
$\tau_s^{(1)}$/ s	$8.67 * 10^{-4}$	$1.07 * 10^{-4}$	$2.15 * 10^{-5}$	$5.20 * 10^{-6}$	$1.41 * 10^{-6}$
β_s	0.40	0.40	0.40	0.40	0.40
$\tau_i^{(1)}$/ s	$8.51 * 10^{-5}$	$1.05 * 10^{-5}$	$2.11 * 10^{-6}$	$5.35 * 10^{-7}$	$1.65 * 10^{-7}$
β_i	0.40	0.40	0.42	0.42	0.42
rel. error (%)	31.2	16.1	14.2	11.1	12.6

enters the frequency window. The parameters characterising the Cole-Davidson susceptibility curves are included in Table 5, while the obtained correlation times are compared in Fig. 8d.

Before we begin the discussion we wish to point out that the purpose of the paper is not to demonstrate an agreement (or a disagreement) between the results obtained from NMR relaxometry

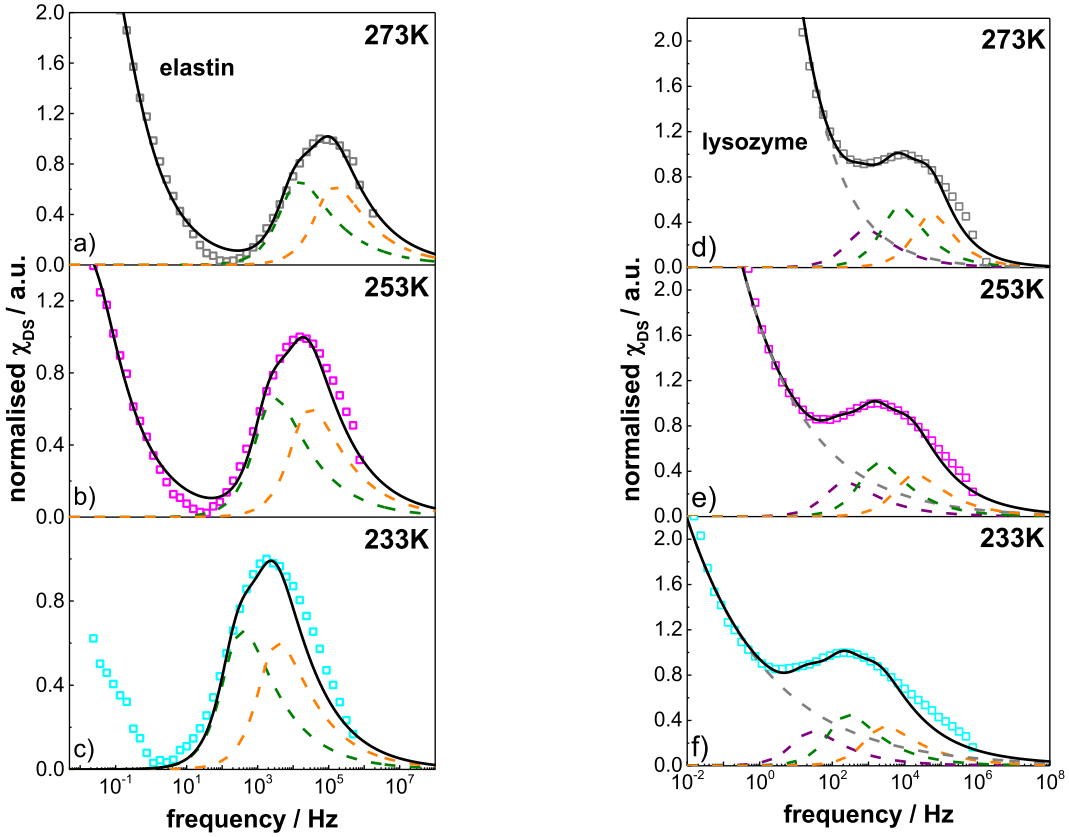

Fig. 7. Normalized dielectric relaxation spectra for elastin at 273 K, 253 K and 233 K for (a), (b), (c) elastin and (d), (e), (f) lysozyme reproduced in terms of Eq. (8) and decomposed into the individual contributions – conductivity (grey dashed line), extra slow process (purple dashed line), slow process (green dashed line) and intermediate process (orange dashed line); black solid lines – overall fits including the conductivity term. (For interpretation of the references to color in this figure legend, the reader is referred to the web version of this article.)

Table 3
Parameters obtained from the analysis of dielectric relaxation spectra for lysozyme. $C_{DS,es}/C_{DS,s}$ = 0.69, $C_{DS,s}/C_{DS,i}$ = 1.23.

T / K	233	253	273
$\tau_{es}^{(1)}$ / s	1.12 * 10^{-2}	1.37 * 10^{-3}	3.21 * 10^{-4}
β_{es}	0.42	0.42	0.50
$\tau_{s}^{(1)}$ / s	1.09 * 10^{-3}	1.48 * 10^{-4}	3.20 * 10^{-5}
β_{s}	0.44	0.48	0.60
$\tau_{i}^{(1)}$ / s	1.15 * 10^{-4}	1.55 * 10^{-5}	3.75 * 10^{-6}
β_{i}	0.40	0.45	0.70
rel. error (%)	11.7	10.6	13.1

and DS. On the basis of the presented data, one is not able to draw ultimate conclusions. The comparison, however, should stimulate a discussion about the mechanisms of motion in proteins (in particular) and analogies between the findings of NMR relaxometry and DS (in general).

In the first step a description of the NMR relaxation profiles and DS relaxation spectra allowing for a comparison of the parameters obtained by reproducing both types of results has been proposed. In both cases the data have been modelled in terms of the same spectral density (susceptibility) forms. Such a comparison would not be possible for a power-law model of the ^{1}H relaxation processes. However, independently of the model, the data clearly show that the dynamics reflected by the ^{1}H relaxation is very similar for all proteins and only weakly dependent on temperature. This does not apply to the DS data. This might bring one to the conclusion that the methods probe different kinds of protein dynamics. At this stage it is worth pointing out that for simple molecules (such as glycerol) [50,51] the agreement between the parameters describing their rotational dynamics obtained by means of NMR relaxometry and DS are in a very good agreement. Coming back to the parameters obtained from the analysis of the NMR relaxation data, one might attribute the slow and intermediate dynamical processes (characterized by the correlation times $\tau_s^{(2)}$ and $\tau_i^{(2)}$) to global motions of whole protein domains leading to conformational changes [38,52], however this statement is hypothetical. Actually, instead of introducing the slow and intermediate processes one could reproduce the ^{1}H relaxation profiles by assuming a distribution of correlation times covering both the contributions. The fast motional process ($\tau_f^{(2)}$) could be associated with dynamics of structural elements, like α-helices [38,53].

Comparing the correlation times obtained by means of NMR and DS for elastin one can get the impression of a relatively good agreement (Figs. 6 and 8a), One can also see from Fig. 6 that the DS relaxation spectra can be reproduced in terms of different models – one can use the Cole-Davidson form of the susceptibility function, but one can also reach this goal by using the correlation times obtained from the analysis of the ^{1}H relaxation data, employing the relationship $\tau_c^{(1)} = 3\tau_c^{(2)}$ and adjusting the amplitudes of the Debye contributions – there is no reason to follow the relationship between the dipolar relaxation constants in the analysis of the dielectric spectra. It is interesting to recognize that the temperature shift in the position of the dielectric spectra (293 K and 312 K, Fig. 5) can be achieved by changing the relative amplitudes of the contributing processes, keeping the correlation times only weakly temperature-dependent (as obtained from the analysis of

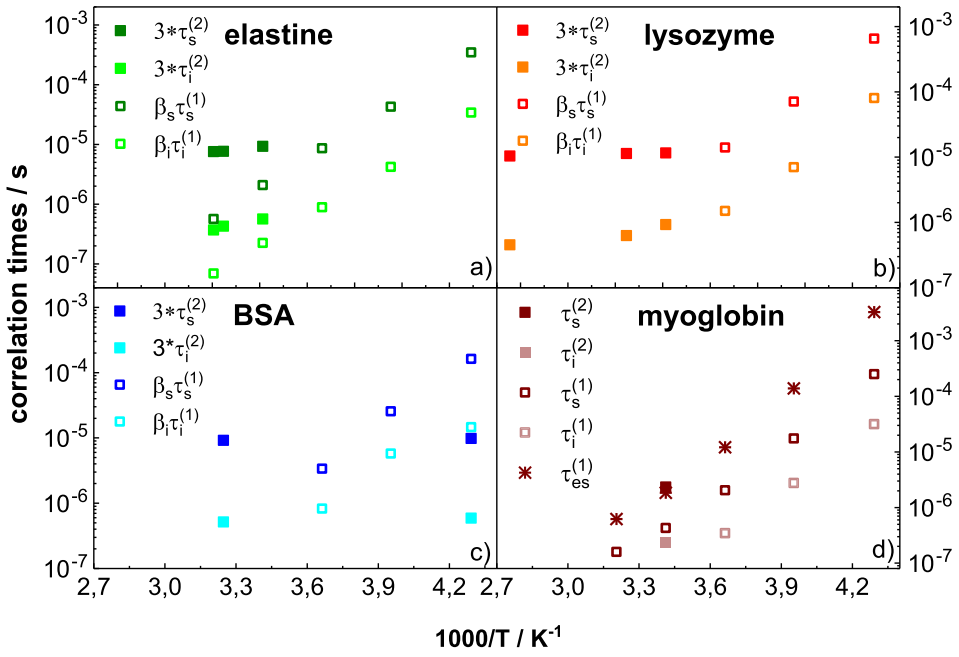

Fig. 8. Comparison of correlation time obtained by means of NMR relaxometry and DS.

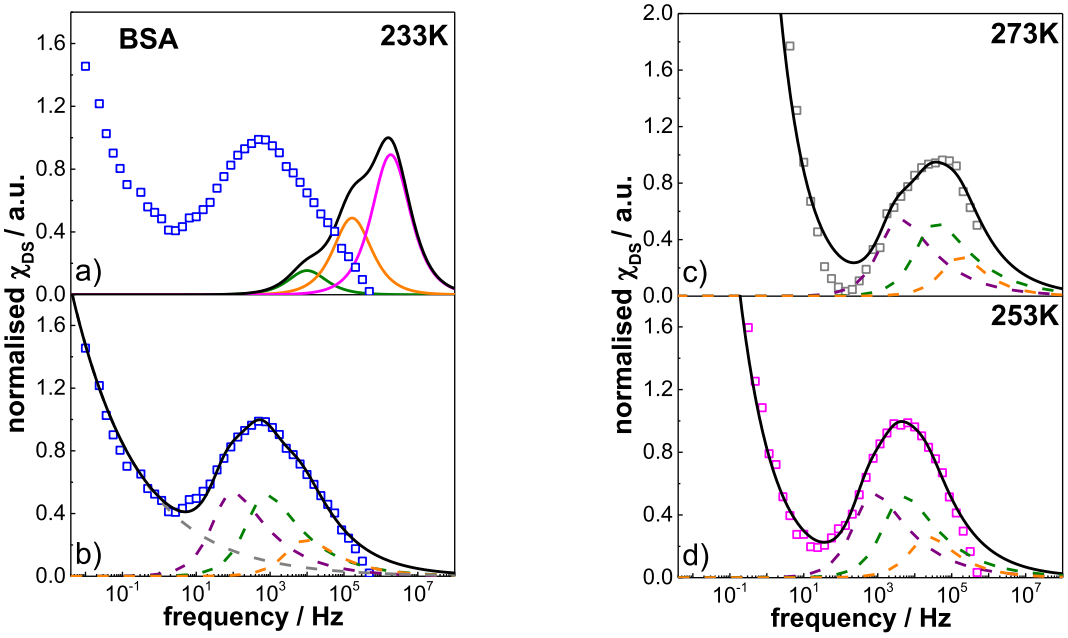

Fig. 9. (a) Normalized dielectric relaxation spectra for BSA at 233 K compared with the$R_1^{HH}(\omega_H)$ relaxation contribution in the susceptibility representation (χ_{NMR}) decomposed into $R_{1,s}^{HH}$ (green solid line), $R_{1,i}^{HH}$ (orange solid line) and$R_{1,f}^{HH}$ (pink solid line) relaxation rates (corresponding to $\chi_{NMR,s}$, $\chi_{NMR,i}$ and $\chi_{NMR,f}$, respectively); (b), (c), (d) normalized dielectric relaxation spectra for BSA at 233 K, 253 K and 273 K reproduced in terms of Eq. (8) and decomposed into the individual contributions – extra slow process (purple dashed line), slow process (green dashed line) and intermediate process (orange dashed line); black solid lines – overall fits. (In (c) and (d)) the conductivity contribution is not explicitly shown, but it is included into the overall fit). (For interpretation of the references to color in this figure legend, the reader is referred to the web version of this article.)

Table 4
Parameters obtained from the analysis of dielectric relaxation spectra for BSA. $C_{DS,es}/C_{DS,s}$ = 1.03, $C_{DS,s}/C_{DS,i}$ = 2.38.

T / K	233	253	273
$\tau_{es}^{(1)}$/ s	3.31 * 10^{-3}	4.05 * 10^{-4}	7.85 * 10^{-5}
β_{es}	0.40	0.40	0.42
$\tau_{s}^{(1)}$/ s	4.05 * 10^{-4}	6.41 * 10^{-5}	8.45 * 10^{-6}
β_{s}	0.40	0.40	0.40
$\tau_{i}^{(1)}$/ s	3.25 * 10^{-5}	1.05 * 10^{-5}	1.31 * 10^{-6}
β_{i}	0.45	0.55	0.63
rel. error (%)	7.9	8.7	10.7

the NMR relaxation data). This strategy can, however, be hardly continued down to 233 K and one might wonder to which extent it is physically justified. The correlation times obtained for lysozyme (Fig. 8b) can be considered as being potentially consistent, provided the dynamics associated with the ^{1}H relaxation slows down with temperature. This effect cannot be excluded, however it has not been observed for BSA (Fig. 8c). As far as the possible mechanisms of the dynamical processes contributing to the DS relaxation spectra are concerned, they are also unknown. In [49] the dielectric peaks for dry lysozyme (being with a good agreement

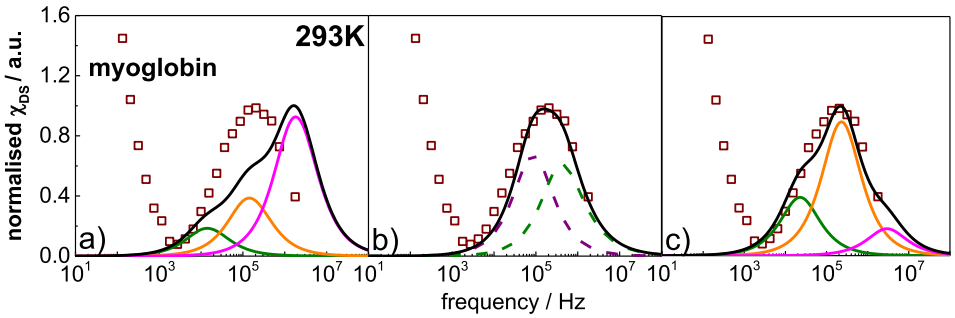

Fig. 10. a) Normalized dielectric relaxation spectrum for myoglobin at 293 K compared with the $R_1^{HH}(\omega_H)$ relaxation contribution in the susceptibility representation (χ_{NMR}) decomposed into $R_{1,s}^{HH}$ (green solid line), $R_{1,i}^{HH}$ (orange solid line) and $R_{1,f}^{HH}$ (pink solid line) relaxation rates (corresponding to $\chi_{NMR,s}$, $\chi_{NMR,i}$ and $\chi_{NMR,f}$, respectively); b) normalized $\chi_{DS}(\omega)$ reproduced in terms of Eq. (8) and decomposed into the individual contributions – extra slow process (purple dashed line), slow process (green dashed line); c) normalized $\chi_{DS}(\omega)$ reproduced as a sum of processes contributing to the $R_1^{HH}(\omega_H)$ relaxation terms ($\beta_s = \beta_i = \beta_f = 1$), but with the adjusted pre-factors – C_s^{HH}/C_i^{HH} = 0.44, C_i^{HH}/C_f^{HH} = 4.97; black solid lines – overall fits. (For interpretation of the references to color in this figure legend, the reader is referred to the web version of this article.)

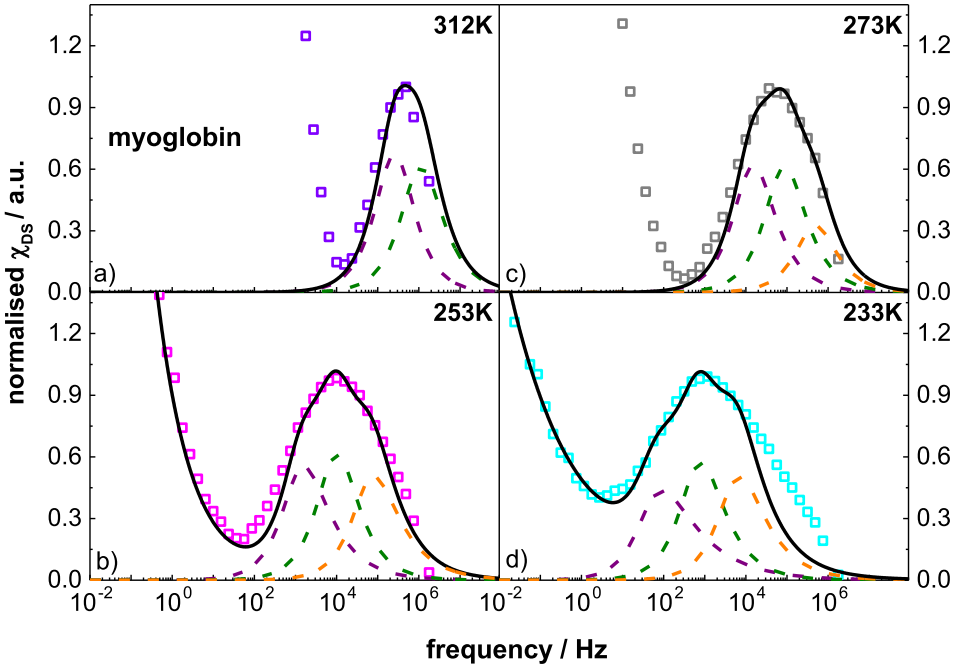

Fig. 11. Normalized dielectric relaxation spectra for myoglobin at 312 K, 273 K, 253 K and 233 K reproduced in terms of Eq. (8) and decomposed into the individual contributions – extra slow process (purple dashed line), slow process (green dashed line) and intermediate process (orange dashed line); black solid lines – overall fits (the conductivity contribution is not explicitly shown, but it is included into the overall fit). (For interpretation of the references to color in this figure legend, the reader is referred to the web version of this article.)

Table 5
Parameters obtained from the analysis of dielectric relaxation spectra for myoglobin. $C_{DS,es}/C_{DS,s}$ = 1.02, $C_{DS,s}/C_{DS,i}$ = 1.07.

T / K	233	253	273	293	312
$\tau_{es}^{(1)}$ / s	$3.28 * 10^{-3}$	$1.39 * 10^{-4}$	$1.21 * 10^{-5}$	$1.84 * 10^{-6}$	$6.21 * 10^{-7}$
β_{es}	0.45	0.67	0.83	1	1
$\tau_s^{(1)}$ / s	$2.50 * 10^{-4}$	$1.75 * 10^{-5}$	$2.05 * 10^{-6}$	$4.29 * 10^{-7}$	$1.59 * 10^{-7}$
β_s	0.75	0.86	0.86	0.86	0.86
$\tau_i^{(1)}$ / s	$3.15 * 10^{-5}$	$2.75 * 10^{-6}$	$3.45 * 10^{-7}$	–	–
β_i	0.66	0.66	0.91	–	–
rel. error (%)	32.1	15.9	13.8	15.3	17.4

with our data) have been attributed to structural relaxation of ill-defined mechanism (the have not been decomposed into individual contributions). For myoglobin the correlation time $\tau_s^{(2)}$ is more close to $\tau_{es}^{(1)}$ than to $\tau_s^{(1)}$ (omitting any scaling).

The overview of the parameters obtained by means of NMR relaxometry and DS can suggest that a significant contribution to the ^{1}H relaxation rates is associated with dynamics that is not probed in DS. The question whether, for instance, fluctuations propagating along the protein backbone can give rise to such a relaxation contribution remains open. In any case, we are of the opinion that the "model-free" approach provides a valuable insight into the protein dynamics, allowing determination of its time scale (that can hardly be obtained in terms of a power-law) and reflecting the heterogeneity of the dynamics.

Eventually, it is very important to broach the subject of the origin of the dielectric spectra in the presence of water. Although the protein powders were lyophilized, they include a small amount of water (this can be concluded from the conductivity contribution). Comparison of DS and neutron scattering results show that the processes observed in DS do not stem just from water. It has been suggested that they can be ascribed to protein's structural relaxation coupled to water and to a large scale protein's motions (e.g., hinge bending, secondary structure, or domain motions) [45]. Moreover, with the support of Molecular Dynamics simulations it has been demonstrated that even for hydrated proteins the DS spectra cannot be assigned only to hydration water [67–69], but they definitely reveal the presence of protein relaxation.

4. Conclusions

^{1}H spin–lattice relaxation and DS studies have been performed for solid Elastin from bovine neck ligament, Lysozyme from hen egg white, BSA and Myoglobin from equine heart in the frequency range of about 10 kHz-40 MHz for NMR relaxometry and 10^{-2}Hz-20 MHz for DS. A theoretical description of the NMR relaxation profiles and DS relaxation spectra has been formulated in a way allowing for a direct comparison of dynamical parameters (correlation times) of motional processes probed by the two methods. It has turned out that the ^{1}H spin–lattice relaxation profiles do not differ much among the proteins and they are only weakly dependent on temperature – consequently, the correlations times obtained by means of NMR relaxometry do not vary much even in a relatively large temperature range. The correlations times are of the order of 10^{-6}s, 10^{-7}s and 10^{-8}s and they have been referred as describing slow, intermediate and fast dynamics, respectively. It has been proposed that the motion of the time scale of 10^{-6}s-10^{-7}s could be ascribed to dynamics of whole protein domains leading to conformational changes, while the motion of the timescale of 10^{-8}s could be attributed to dynamics of structural elements such as α-helices. For the first three proteins QRE effects (quadrupole peaks) have been observed. A thorough analysis of their positions and shapes has led to a determination of the quadrupole parameters at the ^{14}N sites and the orientation of the ^{1}H-^{14}N dipole–dipole axis with respect to the principal axis system of the electric field gradient. Such information cannot be obtained by other methods. The analysis of DS relaxation spectra has also revealed three motional processes referred to as extra-slow, slow and intermediate ones. The assignment has been used merely for the purpose of the discussion, because, in contrast to the correlation times obtained from the analysis of the ^{1}H spin–lattice relaxation data, the DS correlation times considerably depend on temperature. This finding essentially differs from the outcome of a comparison between rotational correlation times obtained by means of NMR relaxometry and DS for simple liquids – in that case the parameters are in a very good agreement [48,49]. In summary, the obtained results suggest that for solid proteins there is a contribution to the ^{1}H spin–lattice relaxation associated with a kind of motion that is not probed in DS as it does not lead to a reorientation of the electric dipole moment.

Declaration of Competing Interest

The authors declare no competing interests.

Acknowledgement

This project has received funding from the European Union's Horizon 2020 research and innovation programme under grant agreement No 668119 (project "IDentIFY").

Appendix A. Supplementary material

Supplementary data to this article can be found online at https://doi.org/10.1016/j.jmr.2020.106721.

References

[1] T. Sugiki, N. Kobayashi, T. Fujiwara, Modern technologies of solution nuclear magnetic resonance spectroscopy for three-dimensional structure determination of proteins open avenues for life scientists, Comput. Struct. Biotechnol. J. 15 (2017) 328–339, https://doi.org/10.1016/j.csbj.2017.04.001.
[2] T. Ikeya, P. Güntert, Y. Ito, Protein structure determination in living cells, Int. J. Mol. Sci. 20 (2019) 2442-1–2442-13. doi:10.3390/ijms20102442.
[3] K. Wüthrich, The way to NMR structures of proteins, Nat. Struct. Biol. 8 (2001) 923–925, https://doi.org/10.1038/nsb1101-923.
[4] F. Fujara, D. Kruk, A.F. Privalov, Solid state Field-Cycling NMR relaxometry: Instrumental improvements and new applications, Prog. Nucl. Magn. Reson. Spectrosc. 82 (2014) 39–69, https://doi.org/10.1016/j.pnmrs.2014.08.002.
[5] R. Kimmich, E. Anoardo, Field-cycling NMR relaxometry, Prog. Nucl. Magn. Reson. Spectrosc. 44 (2004) 257–320, https://doi.org/10.1016/j.pnmrs.2004.03.002.
[6] S.H. Koenig, R.D. Brown, Field-cycling relaxometry of protein solutions and tissue: Implications for MRI, Prog. Nucl. Magn. Reson. Spectrosc. 22 (1990) 487–567, https://doi.org/10.1016/0079-6565(90)80008-6.
[7] R.G. Bryant, D. A. Mendelson. C.C. Lester, The magnetic-field dependence of proton spin relaxation in tissues, Magn. Reson. in Medicine 21 (1991) 117-126. doi: 10.1002/mrm.1910210114.
[8] D. Kruk, A. Herrmann, E.A. Rössler, Field-cycling NMR relaxometry of viscous liquids and polymers, Prog. Nucl. Magn. Reson. Spectrosc. 63 (2012) 33–64, https://doi.org/10.1016/j.pnmrs.2011.08.001.
[9] P.J. Sebastião, Chapter 11: NMR Relaxometry in liquid crystals: Molecular organization and molecular dynamics interrelation. In Field-cycling NMR Relaxometry: Instrumentation, Model Theories and Applications; The Royal Society of Chemistry, London, UK. 2018; pp. 255–302. doi:10.1039/9781788012966-00255.
[10] J.P. Korb, Multi-scales nuclear spin relaxation of liquids in porous media, Comptes Rendus Phys. 11 (2010) 192–203, https://doi.org/10.1016/j.crhy.2010.06.015.
[11] R. Meier, D. Kruk, E.A. Rössler, Intermolecular spin relaxation and translation diffusionin liquids and polymer melts: insight from field-cycling ^{1}H NMR relaxometry, ChemPhysChem 14 (2013) 3071–3081, https://doi.org/10.1002/cphc.201300257.
[12] A. Abragam, The Principles of Nuclear Magnetism, 1st ed., University Press, Oxford, 1961.
[13] C.P. Slichter, Principles of magnetic resonance, 3rd ed., Springer-Verlag, Berlin, 1990.
[14] J. Kowalewski, L. Maler, Nuclear Spin Relaxation in Liquids: Theory, Experiments, and Applications, 2nd ed.;., CRC Press, Taylor & Francis Group: Boca Raton, Florida, FL, USA, 2017.
[15] D. Kruk, Understanding Spin Dynamics, CRC Press, Pan Stanford Publishing, Boca Raton. Florida FL, 2015.
[16] P.-O. Westlund, Quadrupole-enhanced proton spin relaxation for a slow reorienting spin pair: (I)–(S). A stochastic Liouville approach, Mol. Phys. 107 (2009) 2141–2148, https://doi.org/10.1080/00268970903185909.
[17] P.-O. Westlund, The quadrupole enhanced ^{1}H spin-lattice relaxation of the amide proton in slow tumbling proteins, PCCP 12 (2010) 3136–3140, https://doi.org/10.1039/b922817a.
[18] D. Kruk, A. Kubica, W. Masierak, A.F. Privalov, M. Wojciechowski, W. Medycki, Quadrupole relaxation enhancement–application to molecular crystals, Solid State Nucl. Magn. Reson. 40 (2011) 114–120, https://doi.org/10.1016/j.ssnmr.2011.08.003.
[19] D. Kruk, E. Umut, E. Masiewicz, R. Fischer, H. Scharfetter, Multi-quantum quadrupole relaxation enhancement effects in 209Bi compounds, J. Chem. Phys. 150 (2019) 184309-1–184309-8. doi:10.1063/1.5082007.
[20] D. Kruk, A. Privalov, W. Medycki, C. Uniszkiewicz, W. Masierak, R. Jakubas, NMR studies of solid-state dynamics, in annual reports on NMR spectroscopy, Elsevier Ltd, Amsterdam, Netherlands 76 (2012) 67–138, https://doi.org/10.1016/B978-0-12-397019-0.00003-0.
[21] M. Florek-Wojciechowska, M. Wojciechowski, R. Jakubas, S. Brym, D. Kruk, 1H NMR relaxometry and quadrupole relaxation enhancement as a sensitive probe of dynamical properties of solids—[C(NH2)3]3Bi2I9 as an example, J. Chem. Phys. 144 (2016) 054501-1–054501-8. doi:10.1063/1.4940680.
[22] M. Florek-Wojciechowska, R. Jakubas, D. Kruk, Structure and dynamics of $[NH_2(CH_3)_2]_3Sb_2Cl_9$ by means of ^{1}H NMR relaxometry – quadrupolar relaxation enhancement effects, PCCP 19 (2017) 11197–11205, https://doi.org/10.1039/c7cp00788D.
[23] D. Kruk, E. Umut, E. Masiewicz, C. Sampl, R. Fischer, S. Spirk, C. Gösweiner, H. Scharfetter, 209 Bi quadrupole relaxation enhancement in solids as a step towards new contrast mechanisms in magnetic resonance imaging, PCCP 20 (2018) 12710–12718, https://doi.org/10.1039/C8CP00993g.
[24] D. Kruk, W. Medycki, A. Mielczarek, R. Jakubas, C. Uniszkiewicz, Complex nuclear relaxation processes in guanidinium compounds $[C(NH_2)_3]_3Sb_2X_9$ (X = Br, Cl): effects of quadrupolar interactions, Appl. Magn. Reson. 39 (2010) 233–249, https://doi.org/10.1007/s00723-010-0152-x.

[25] E.P. Sunde, B. Halle, Mechanism of ^{1}H–^{14}N cross-relaxation in immobilized proteins, J. Magn. Reson. 203 (2010) 257–273, https://doi.org/10.1016/j.jmr.2010.01.008.

[26] F. Winter, R. Kimmich, $^{14}N^{1}H$ and $^{2}H^{1}H$ cross-relaxation in hydrated proteins, Biophys. J . 48 (1985) 331–335, https://doi.org/10.1016/S0006-3495(85)83787-5.

[27] D.J. Lurie, Quadrupole-Dips Measured by Whole-Body Field-Cycling Relaxometry and Imaging, in: Proc. Int. Soc. Magn. Reson. Med.7 (1999) 653.

[28] D.J. Lurie, G.R. Davies, M.A. Foster, J.M.S.S. Hutchison, Field-cycled PEDRI imaging of free radicals with detection at 450 mT, Magn. Reson. Imaging 23 (2005) 175–181, https://doi.org/10.1016/j.mri.2004.11.051.

[29] D.J. Lurie, S. Aime, S. Baroni, N.A. Booth, L.M. Broche, C.-H. Choi, G.R. Davies, S. Ismail, D. Ó hÓgáin, K.J. Pine, Fast field-cycling magnetic resonance imaging, Comptes Rendus Phys. 11 (2010) 136–148. doi:10.1016/j.crhy.2010.06.012.

[30] Y.A. Goddard, J.P. Korb, R.G. Bryant, Water molecule contributions to proton spin-lattice relaxation in rotationally immobilized proteins, J. Magn. Reson. 199 (2009) 68–74, https://doi.org/10.1016/j.jmr.2009.04.001.

[31] J.P. Korb, R.G. Bryant, Magnetic field dependence of proton spin-lattice relaxation of confined proteins, Comptes Rendus Phys. 5 (2004) 349–357, https://doi.org/10.1016/j.crhy.2004.03.001.

[32] C.C. Lester, R.G. Bryant, Water–proton nuclear magnetic relaxation in heterogeneous systems: hydrated lysozyme results, Magn. Reson. Med. 22 (1991) 143–153, https://doi.org/10.1002/mrm.1910220115.

[33] R.G. Bryant, The dynamics of water-protein interactions, Annu. Rev. Biophys. Biomol. Struct. 25 (1996) 29–53, https://doi.org/10.1146/annurev.bb.25.060196.000333.

[34] I. Bertini, M. Fragai, C. Luchinat, G. Parigi, ^{1}H NMRD profiles of diamagnetic proteins: a model-free analysis, Magn. Reson. Chem. 38 (2000) 543–550, https://doi.org/10.1002/1097-458X(200007)38:7<543::AID-MRC722>3.0.CO;2-%23.

[35] E. Ravera, G. Parigi, A. Mainz, T.L. Religa, B. Reif, C. Luchinat, Experimental determination of microsecond reorientation correlation times in protein solutions, J. Phys. Chem. B 117 (2013) 3548–3553, https://doi.org/10.1021/jp312561f.

[36] J.P. Korb, A. Van-Quynh, R. Bryant, Low-frequency localized spin-dynamical coupling in proteins, Comptes Rendus l'Academie Des Sci.–Ser. IIc Chem. 4 (2001) 833–837. doi:10.1016/S1387-1609(01)01323-8.

[37] Y. Goddard, J.P. Korb, R.G. Bryant, The magnetic field and temperature dependences of proton spin-lattice relaxation in proteins, J. Chem. Phys. 126 (2007) 175105-1 – 175105-5. doi:10.1063/1.2727464.

[38] D. Kruk, E. Masiewicz, A.M. Borkowska, P. Rochowski, P.H. Fries, L.M. Broche, D. J. Lurie, Dynamics of Solid Proteins by Means of Nuclear Magnetic Resonance Relaxometry, Biomolecules. 9 (2019) 652-1 – 652-13. doi:10.3390/biom9110652.

[39] B. Halle, H. Jóhannesson, K. Venu, Model-free analysis of stretched relaxation dispersions, J. Magn. Reson. 135 (1998) 1–13, https://doi.org/10.1006/jmre.1998.1534.

[40] C. Luchinat, G. Parigi, E. Ravera, Water and protein dynamics in sedimented systems: a relaxometric investigation, ChemPhysChem 14 (2013) 3156–3161, https://doi.org/10.1002/cphc.201300167.

[41] E. Ravera, M. Fragai, G. Parigi, C. Luchinat, differences in dynamics between crosslinked and non-crosslinked hyaluronates measured by using fast field-cycling relaxometry, ChemPhysChem 16 (2015) 2803–2809, https://doi.org/10.1002/cphc.201500446.

[42] A. Panagopoulou, A. Kyritsis, M. Vodina, P. Pissis, Dynamics of uncrystallized water and protein in hydrated elastin studied by thermal and dielectric techniques, Biochim. Biophys. Acta – Proteins Proteomics. 2013 (1834) 977–988, https://doi.org/10.1016/j.bbapap.2013.03.015.

[43] V. Samouillan, A. Lamure, C. Lacabanne, Dielectric relaxations of collagen and elastin in the dehydrated state, Chem. Phys. 255 (2000) 259–271, https://doi.org/10.1016/S0301-0104(00)00080-X.

[44] S. Khodadadi, S. Pawlus, J.H. Roh, V. Garcia Sakai, E. Mamontov, A.P. Sokolov, The origin of the dynamic transition in proteins, J. Chem. Phys. 128 (2008) 195106-1–195106-5. doi:10.1063/1.2927871.

[45] S. Khodadadi, S. Pawlus, A.P. Sokolov, Influence of hydration on protein dynamics: combining dielectric and neutron scattering spectroscopy data, J. Phys. Chem. B 112 (2008) 14273–14280, https://doi.org/10.1021/jp8059807.

[46] M. Nakanishi, A.P. Sokolov, Protein dynamics in a broad frequency range: dielectric spectroscopy studies, J. Non-Cryst. Solids 407 (2015) 478–485, https://doi.org/10.1016/j.jnoncrysol.2014.08.057 0022-3093.

[47] K.L. Ngai, S. Capaccioli, S. Ancherbak, N. Shinyashiki, Resolving the ambiguity of the dynamics of water and clarifying its role in hydrated proteins, Phil. Mag. 91 (2011) 1809–1835, https://doi.org/10.1080/14786435.2010.523716.

[48] K.L. Ngai, S. Capaccioli, A. Paciorani, Dynamics of hydrated proteins and bio-protectants: caged dynamics, β-relaxation, and α-relaxation, BBA 2017 (1861) 3553–3563, https://doi.org/10.1016/j.bbagen.2016.04.027.

[49] K. Sasaki, I. Popov, Y. Feldman, Water in the hydrated protein powders: dynamic and structure, J. Chem. Phys. 150 (2019), https://doi.org/10.1063/1.5096881 204504.

[50] D. Kruk, R. Meier, E.A. Rössler, Translational and rotational diffusion of glycerol by means of field cycling 1H NMR relaxometry, J. Phys. Chem. B 115 (2011) 951–957, https://doi.org/10.1021/jp110514r.

[51] R. Meier, R. Kahlau, D. Kruk, E.A. Rössler, Comparative studies of the dynamics in viscous liquids by means of dielectric spectroscopy and field cycling NMR, J. Phys. Chem. A 114 (2010) 7847–7855, https://doi.org/10.1021/jp102498q.

[52] P.H. Fries, E. Belorizky, Simple expressions of the nuclear relaxation rate enhancement due to quadrupole nuclei in slowly tumbling molecules, J. Chem. Phys. 143 (2015) 044202–1 - 044202-17. doi:10.1063/1.4926827.

[53] C.P. Lindsey, G.D. Patterson, Detailed comparison of the williams-watts and cole-davidson functions, J. Chem. Phys. 73 (1980) 3348–3357, https://doi.org/10.1063/1.440530.

[54] R. Kahlau, D. Kruk, T. Blochowicz, V.N. Novikov, E.A. Rössler, Generalization of the Cole-Davidson and Kohlrausch functions to describe the primary response of glass-forming systems, J. Phys. Condens. Matter 22 (2010) 365101-1-365101-8. doi: 10.1088/0953-8984/22/36/365101.

[55] S. Havriliak, S. Negami, A complex plane representation of dielectric and mechanical relaxation processes in some polymers, Polymer 8 (1967) 161–210, https://doi.org/10.1016/0032-3861(67)90021-3.

[56] R. Feng, Y. Konishi, A.W. Bell, High accuracy molecular weight determination and variation characterization of proteins up to 80 ku by ionspray mass spectrometry, J. Am. Soc. Mass Spectrom. 2 (1991) 387–401, https://doi.org/10.1016/1044-0305(91)85005-Q.

[57] K.A. Majorek, P.J. Porebski, A. Dayal, M.D. Zimmerman, K. Jablonska, A.J. Stewart, M. Chruszcz, W. Minor, Structural and immunologic characterization of bovine, horse, and rabbit serum albumins, Mol. Immunol. 52 (52) (2012) 174–182, https://doi.org/10.1016/j.molimm.2012.05.011.

[58] K. V. Abrosimova, O. V. Shulenina, S. V. Paston, FTIR study of secondary structure of bovine serum albumin and ovalbumin. J. Phys. Conf. Ser. (2016) 769, 012016-1 – 012016-6. doi: 10.1088/1742-6596/769/1/012016.

[59] K.J. Palmer, M. Ballantyne, J.A. Galvin, The molecular weight of lysozyme determined by the x-ray diffraction method, J. Am. Chem. Soc. 70 (1948) 906–908, https://doi.org/10.1021/ja01183a007.

[60] F.H. White, Studies on secondary structure in chicken egg-white lysozyme after reductive cleavage of disulfide bondst, Biochemistry 15 (1976) 2906–2912, https://doi.org/10.1021/bi00658a032.

[61] L. Debelle, A.J.P. Alix, S.M. Wei, M.P. Jacob, J.P. Huvenne, M. Berjot, P. Legrand, The secondary structure and architecture of human elastin, Eur. J. Biochem. 258 (1998) 533–539, https://doi.org/10.1046/j.1432-1327.1998.2580533.x.

[62] F.W. Keeley, C.M. Bellingham, K.A. Woodhouse, Elastin as a self-organizing biomaterial: use of recombinantly expressed human elastin polypeptides as a model for investigations of structure and self-assembly of elastin, Philos. Trans. R. Soc. B Biol. Sci. 357 (2002) 185–189, https://doi.org/10.1098/rstb.2001.1027.

[63] G.A. Ordway, D.J. Garry, Myoglobin: an essential hemoprotein in striated muscle, J. Exp. Biol. 207 (2004) 3441–3446, https://doi.org/10.1242/jeb.01172.

[64] J.P. Collman, J.I. Brauman, T.R. Halbert, K.S. Suslick, Nature of O_2 and CO binding to metalloporphyrins and heme proteins, Proc Natl Acad Sci USA 73 (1976) 3333–3337.

[65] Y. Goddard, J-P. Korb, R. Bryant, The magnetic field and temperature dependences of proton spin-lattice relaxation in proteins, J. Chem. Phys. 126 (2007) 75105-1- 75105-5. doi: https://doi.org/10.1063/1.2727464.

[66] L. Yao, B. Vögeli, J. Ying, A. Bax, NMR determination of amide N-H equilibrium bond length from concerted dipolar coupling measurements, J. Am. Chem. Soc. 130 (2008) 16518–16520, https://doi.org/10.1021/ja805654f.

[67] J. Guo, H.-X. Zhou, Protein allostery and conformational dynamics, Chem. Rev. 116 (2016) 6503–6515, https://doi.org/10.1021/acs.chemrev.5b00590.

[68] Y. Xu, M. Havenith, Perspective: Watching low-frequency vibrations of water in biomolecular recognition by THz spectroscopy, J. Chem. Phys. 143 (2015) 170901-1–170901-7. doi:10.1063/1.4934504.

[69] S. Khodadadi, E. Curtis, A.P. Sokolov, Nanosecond relaxation dynamics of hydrated proteins: water versus protein contributions, J. Phys. Chem. B 115 (2011) 6222–6226, https://doi.org/10.1021/jp1122213.